

Aeroelasticity using level set approach and adaptive mesh

Ghalia Guiza

▶ **To cite this version:**

Ghalia Guiza. Aeroelasticity using level set approach and adaptive mesh. [Research Report] Ecole Nationale Supérieure des Mines de Paris. 2016, pp.19. hal-01492607

HAL Id: hal-01492607

https://minesparis-psl.hal.science/hal-01492607

Submitted on 20 Mar 2017

HAL is a multi-disciplinary open access archive for the deposit and dissemination of scientific research documents, whether they are published or not. The documents may come from teaching and research institutions in France or abroad, or from public or private research centers.

L'archive ouverte pluridisciplinaire **HAL**, est destinée au dépôt et à la diffusion de documents scientifiques de niveau recherche, publiés ou non, émanant des établissements d'enseignement et de recherche français ou étrangers, des laboratoires publics ou privés.

ECOLE NATIONALE SUPERIEURE DES MINES DE PARIS
CENTRE DE MISE EN FORME DES MATERIAUX





Aeroelasticity using level set approach and adaptive mesh

Ghalia GUIZA

June 23,2016

We have present a full Eulerian approach to deal with the aerodynamic performance and stability of a new designed airship. It consists first on setting the needed fluid solvers (Navier-Stokes equations coupled to a Spallart almaras turbulent model), then on a geometric representation through a level set method that separates each phase: external air, membrane and internal gaz. Finally, we extend this framework to embed a fluid-membrane model through interfacial forces. This model consists on implementing bending and inextensibility forces and adding them to the Navier-sotek equations. The framework was tested first in 3D to analyze the flow past a fixed airship and compute the aerodynamic forces. Then a fluid-membrane benchmark is used to validate the implementation. This work allows us to highlight several numerical challenges: first, the implementation of a high order derivative using smooth projection is needed to ensure free-oscillation forces, then the use of an unified compressible-incompressible solver to take into account the internal gaz of the the airship, finally, the analysis of the envelop proposed by Thales Alenia Space to deduce the physical parameters for our fluid-membrane model.

Contents

1 Introduction **1**

2 Governing equations **2**
2.1 The Navier-Stokes equations 2
2.2 The Spalart-Allmaras turbulence model (SA) 3
2.3 Eulerian framework using a Level set method 5

3 Membrane model **7**
3.1 Bending Force 7
3.2 Inextensibility Force 7
3.3 Discretization 8

4 Numerical experiments **9**
4.1 Flow past a 3D airship 9
4.2 Fluid-membrane test case 11

5 High order derivative by smooth projections **14**

6 Conclusion **15**

1 Introduction

The fluid-structure interaction problem is one of the most active areas of research in numerical simulation in the coming years. The immediate and potential applications include the vast majority of industrial, social and environmental domains. The simulation of fluid-structure interaction is made possible by the considerable progress of computer and technological resources but also by the maturity of the numerical methods for the study of complex physical systems involving laminar or turbulent fluids and rigid or flexible structures. There is a significant number of applications within this theme, particularly in the fields of civil engineering (bridges, towers), medicine (blood flow in the arteries) or aeronautics (flow around airships). In practice, different calculation codes are used to model this interaction, which must be both robust, accurate but also ensuring the conservation of energy and the data relating to the structure, the fluid and the interface resolution. The results of the numerical simulation, especially its stability and accuracy, depend strongly on the parameters, the physical characteristics of the model chosen, the methods and algorithms used.

The project SRATOBUS, the subject of this thesis, aim to study the stability of a new airship, operating at an altitude of about 20 kilometers (halfway between satellites and drones) that can be able to carry payloads up to 250 kg and provide 5 kW of power. It will cover a wide range of missions such as the surveillance of borders or high-value sites, , security (the fight against terrorism, drug trafficking, etc.), environmental monitoring (forest fires, soil erosion, pollution, etc.) and telecommunications (Internet. This airship, as shown in 1, is 100 meters long, 33 meters maximum diameter, and offer a lifespan in the stratosphere of five years.

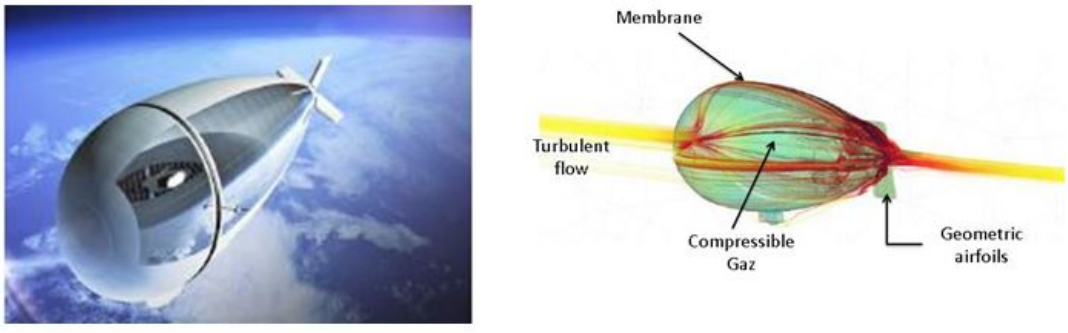


Figure 1: The airship Stratobus

Recall that the subject of this thesis is to analyze the performance of each design and to study the performance of the airship in an extreme environment. Therefore, three main subjects will be treated along the PhD thesis:

• **Aerodynamic**: simulation of turbulent flows past different design and shapes of the airship

• **Aerothermal**: simulation mainly of natural convection and temperature variations
• **Aeroelasticity**: simulation of the fluid - envelope interaction

In this report, we started to cover the first and the third points. Indeed, the turbulent flow past the airship will induce aerodynamic forces on the hull of the airship, which in return will or may deform its envelope. Such simulation is very challenging due to the difference in scale; the thickness of the envelope is around $5cm$. Therefore, we start by setting the first 3D simulation of the flow past the new designed airship, proposed by Thales Alenia Space, then we highlight the advantages and perspectives of the existing fluid mechanics solvers, and finally we study the implementation of a new fluid-membrane numerical method. Inspired from biomechanics applications, we propose here to model an immersed membrane in an incompressible fluid through interfacial forces. Different experimental, numerical and theoretical studies were proposed on this subject [1, 2, 3, 4, 5, 6]. We mainly focused and implemented the orginal idea introduced first by [7] and completed later by [8, 9, 10].

2 Governing equations

In this section, we briefly present the governing equations, namely the unsteady incompressible Navier-Stokes equations coupled to the Spalart-Allmaras turbulence model, and their discretization. We first recall the stabilized Finite Element scheme for the Navier-Stokes equations derived from a variational multiscale point of view where both the velocity and the pressure fields are decomposed into coarse and small scale [11, 12, 13, 14]. The static condensation for the small scale into the large scale will provide additional terms to the Galerkin formulation. These terms allow to cure the spurious oscillations in the convection-dominated regime and to deal with the pressure instability. Second, we recall the stabilized Finite Element scheme for the Spalart-Allmaras transport equation [15] derived simply from the Streamline Upwind Petrov-Galerkin (SUPG) method [16].

2.1 The Navier-Stokes equations

To fix notations, let $\Omega \subset \mathbb{R}^d$ be the fluid domain, where d is the space dimension, and $\partial\Omega$ its boundary. The strong form of the incompressible Navier Stokes equations reads:

$$\begin{cases} \rho\ (\partial_t \mathbf{v} + \mathbf{v} \cdot \nabla \mathbf{v}) - \nabla \cdot \boldsymbol{\sigma} = \mathbf{F} \\ \nabla \cdot \mathbf{v} = 0 \end{cases} \tag{1}$$

where $t \in [0, T]$ is the time, $\mathbf{v}(\mathbf{x}, t)$ the velocity, $p(\mathbf{x}, t)$ the pressure and ρ the density. F plays here an important role, taking into acocunt the forces of the membrane. Its expression will be detailed in section 3. The Cauchy stress tensor for a Newtonian fluid is given by:

$$\boldsymbol{\sigma} = 2\mu\ \boldsymbol{\epsilon}(\mathbf{v}) - p\ \mathbf{I}_d, \tag{2}$$

with $\mathbf{I}_d$ the d-dimensional identity tensor and μ the dynamic viscosity.

The weak form of problem (1) combined with (2) is obtained by multiplication of a test function and integration by parts and reads, under the assumption of homogeneous Dirichlet boundary conditions:

$$\begin{cases} \text{Find } (\mathbf{v}, p) \in V \times Q \text{ such that:} \\ \rho\ [(\partial_t \mathbf{v}, \mathbf{w}) + (\mathbf{v} \cdot \nabla \mathbf{v}, \mathbf{w})] + (2\mu \boldsymbol{\epsilon}(\mathbf{v}) : \boldsymbol{\epsilon}(\mathbf{w})) - (p, \nabla \cdot \mathbf{w}) = (\mathbf{f}, \mathbf{w}), \quad \forall \mathbf{w} \in V \\ (\nabla \cdot \mathbf{v}, q) = 0, \quad \forall q \in Q. \end{cases} \tag{3}$$

where ρ and μ are the density and the dynamic viscosity, respectively. Based on a mesh $\mathcal{K}_h$ of Ω made of N_{el} elements K, the functional spaces for the velocity V and for the pressure Q are approximated by the finite dimensional spaces V_h and Q_h respectively. It is well known that the stability of this formulation requires an appropriate choice of the finite element spaces V_h and Q_h, that must to fulfil a compatibility condition[17]. Accordingly, the standard Galerkin method with the P1/P1 element (i.e. the same piecewise linear space for V_h and Q_h) is not stable. Moreover, convection-dominant problems lead to numerical oscillations that pollute the solution. As menstioned previously, we use a Variational MultiScale method [18] which circumvents both problems through a Petrov-Galerkin approach. The basic idea is to consider that the unknowns can be split into two components, a coarse one and a fine one, corresponding to different scales or levels of resolution. First, we solve the fine scales in an approximate manner and then we replace their effect into the large-scale equation. We present the final obtained variational formulation of the method, and the reader is referred to [19] for extensive details:

$$\begin{cases} \rho\,(\partial_t \mathbf{v}_h, \mathbf{w}_h)_\Omega + (\rho \mathbf{v}_h \cdot \nabla \mathbf{v}_h, \mathbf{w}_h)_\Omega \\ \qquad - \sum_{K \in \mathcal{T}_h} (\tau_1 \boldsymbol{\mathcal{R}}_{\mathrm{M}}, \rho \mathbf{v}_h \nabla \mathbf{w}_h)_K + (2\mu \boldsymbol{\varepsilon}(\mathbf{v}_h) : \boldsymbol{\varepsilon}(\mathbf{w}_h))_\Omega \\ \qquad - (p_h, \nabla \cdot \mathbf{w}_h)_\Omega + \sum_{K \in \mathcal{T}_h} (\tau_2 \mathcal{R}_{\mathrm{C}}, \nabla \cdot \mathbf{w}_h)_K = (\mathbf{f}, \mathbf{w}_h)_\Omega, \quad \forall \mathbf{w}_h \in V_{h,0} \\ (\nabla \cdot \mathbf{v}_h, q_h)_\Omega - \sum_{K \in \mathcal{T}_h} (\tau_1 \boldsymbol{\mathcal{R}}_{\mathrm{M}}, \nabla q_h)_K = 0, \quad \forall q_h \in Q_h \end{cases} \tag{4}$$

where $(\cdot, \cdot)_\Omega$ represents the scalar product on the whole domain omega while $(\cdot, \cdot)_K$ is the scalar product on Element K. The quantities τ_1 and τ_2 are stabilization parameters, $\boldsymbol{\mathcal{R}}_{\mathrm{M}}$ and $\mathcal{R}_{\mathrm{C}}$ are the momentum and the continuity residuals (see [19] for details).

2.2 The Spalart-Allmaras turbulence model (SA)

The range of velocity of the airship is between $20m/s$ and $50m/s$. Based on the length of the airship, the Reynolds number may reach 10^7. To solve accurately such high Reynolds number flows, it requires an extensive number of nodes, in particular at the boundary layers. This is not affordable using the existing resources. Therefore, as is the case in many industrial applications, we refer to the use of the Reynolds-Averaged Navier-Stokes (RANS) equations. They are obtained by applying a time-averaging procedure to the Navier-Stokes equations, which gives rise to an additional stress term (the Reynolds stress tensor) and a turbulent eddy viscosity μ_{t} taking into account the effect of turbulent fluctuations on the averaged flow. Different turbulent model to compute the eddy viscosity μ_{t} exists in the

literature. We choose for this work the one-equation Spalart-Allmaras turbulence model because it is well adapted for external aerodynamic flows [15]. It represents the evolution of the kinematic eddy viscosity $\tilde{\nu}$ by a non linear advection-diffusion-reaction type of equation.

The coupling with the Navier-Stokes equations (4) will be through the velocity field from one side and the eddy viscosity from the other side.

A stabilized Finite Element discretization of the Spallart-Allmaras model and a simple linearisation method were proposed in [20]. Therefore, we follow the same idea, and we write the variational formulation combined with a backward Euler time discretization:

$$\frac{\tilde{\nu}^{n+1}-\tilde{\nu}^{n}}{\Delta t}+\underbrace{\left(\mathbf{v}^{n+1}-\frac{c_{b2}}{\sigma}\nabla\tilde{\nu}^{n+1}\right)\cdot\nabla\tilde{\nu}^{n+1}}_{\text{convection}}-\underbrace{\frac{1}{\sigma}\nabla\cdot\left[(\nu+\tilde{\nu}^{n+1})\nabla\tilde{\nu}^{n+1}\right]}_{\text{diffusion}}$$
$$-\underbrace{\left[c_{b1}(1-f_{t2}^{n+1})\tilde{S}^{n+1}+\left(c_{w1}f_{w}^{n+1}-\frac{c_{b1}}{\kappa^{2}}f_{t2}^{n+1}\right)\frac{\tilde{\nu}^{n+1}}{d^{2}}\right]\tilde{\nu}^{n+1}}_{\text{reaction}}=0, \quad (5)$$

where $\tilde{\nu}^n$ stands for the value of $\tilde{\nu}$ at discrete time t_n. The eddy viscosity can then be obtained from $\mu_t = \rho\tilde{\nu}f_{v1}$, with f_{v1} a damping function, S the turbulent production, d is the shortest distance to the wall, and all the remaining terms are the model specified coefficients (see [15] for details).

Finally by applying a simpler Picard-like linearization [20] and the Streamline Upwind Petrov-Galerkin (SUPG) method, the final weak form of equation (5) reads:

$$\left(\frac{\tilde{\nu}^{n+1,i+1}-\tilde{\nu}^{n}}{\Delta t},\omega_h\right)_\Omega+$$
$$\left(\left[\mathbf{v}^{n+1}-\frac{c_{b2}}{\sigma}\nabla\tilde{\nu}^{n+1,i}\right]\cdot\nabla\tilde{\nu}_h^{n+1,i+1},\omega_h\right)_\Omega-\left(\frac{1}{\sigma}(\nu+\tilde{\nu}_h^{i})\nabla\tilde{\nu}_h^{n+1,i+1},\nabla\omega_h\right)_\Omega$$
$$-\left(\left[c_{b1}(1-f_{t2}^{n+1})\tilde{S}_h^{n+1}+\left(c_{w1}f_{w}^{n+1}-\frac{c_{b1}}{\kappa^{2}}f_{t2}^{n+1}\right)\frac{\tilde{\nu}_h^{n+1,i}}{d^{2}}\right]\tilde{\nu}_h^{n+1,i+1},\omega_h\right)_\Omega$$
$$+\sum_K\left(\mathcal{R}(\tilde{\nu}^{n+1,i}),\tau_3^{n+1,i}\left[\mathbf{v}_h^{n+1}-\frac{c_{b2}}{\sigma}\nabla\tilde{\nu}_h^{n+1,i}\right]\cdot\nabla\omega_h\right)_K=0,\quad\forall\omega_h\in W_h. \quad (6)$$

where $\mathcal{R}(\tilde{\nu})$ is the finite element residual of (5). The stabilization parameter τ_3, is computed within each element as:

$$\tau_3=\left(\frac{c_2}{h}\|\alpha_c\|_K+\frac{c_1}{h_K^2}\alpha_d+\alpha_r\right)^{-1} \quad (7)$$

where α_c, α_d and α_r are respectively the convection, diffusion and reaction coefficients in Equation (6), h_K is the element size, $\|\alpha_c\|_K$ a characteristic norm of the convection term and $c_1 = 4$, $c_2 = 2$ for linear elements.

2.3 Eulerian framework using a Level set method

The level set method [21, 22, 23] defines a signed distance function ϕ as follows:

$$\phi(X) = \begin{cases} -dist(X,\Gamma) & if\ X \in \Omega_1 \\ 0 \quad if\ X \in \Gamma \\ dist(X,\Gamma) & if\ X \in \Omega_2 \end{cases} \tag{8}$$

To restrict and sharpen the interface, we modify, filter and replace the level-set function as follows:

$$\phi(X) = \begin{cases} 2E/\pi & \text{for } \phi > E \\ \dfrac{2E}{\pi}\sin\left(\dfrac{\pi}{2E}\phi\right) & \text{for } |\phi| < E \\ -2E/\pi & \text{for } \phi < -E \end{cases} \tag{9}$$

where E stands for the truncation thickness as shown in 2. Here, the membrane is denoted by Γ and thus decomposes the whole domain into two sub-domains Ω_1 and Ω_2 such that $\Omega = \Omega_1 \cup \Omega_2$. Recall also that as a signed distance function, ϕ has the property $|\nabla\phi| = 1$.

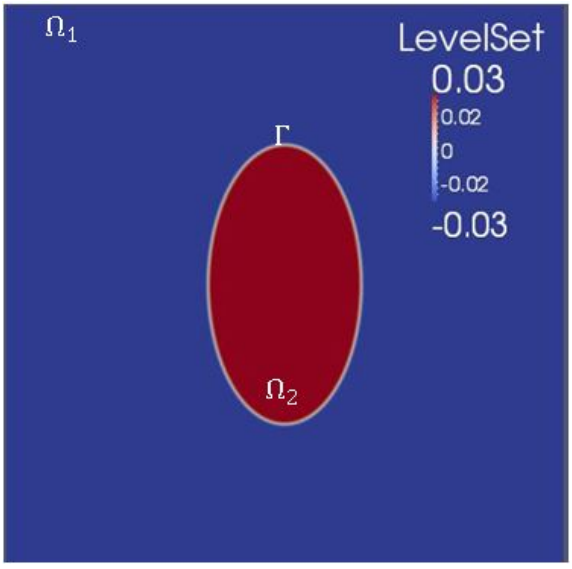


Figure 2: Sign of ϕ

Moreover, we define the smoothed versions of the heaviside and Dirac functions as :

$$H_\varepsilon(\phi) = \begin{cases} 0, & \phi \le -\varepsilon, \\ \frac{1}{2}\left(1 + \frac{\phi}{\varepsilon} + \frac{\sin(\frac{\pi\phi}{\varepsilon})}{\pi}\right), & -\varepsilon \le \phi \le \varepsilon, \\ 1, & \phi \ge \varepsilon, \end{cases} \tag{10}$$

$$\delta_\varepsilon(\phi) = \begin{cases} 0, & \phi \le -\varepsilon, \\ \frac{1}{2\varepsilon}(1 + cos(\frac{\pi\phi}{\varepsilon})), & -\varepsilon \le \phi \le \varepsilon, \\ 0, & \phi \ge, \end{cases} \tag{11}$$

Where ε a numerical parameter that defines the thickness of the interface and taken a value founded in the literature as ($\varepsilon = 1.5h$) with h the mesh size. The Heaviside function is used to determine material values at each point in the domain. For example, let's take the density (ρ_1, ρ_2) and the viscosity (μ_1, μ_2) respectively for (Ω_1, Ω_2) :

$$\rho = \rho_1 + (\rho_2 - \rho_1) H_\varepsilon(\phi) \tag{12}$$

$$\mu = \mu_1 + (\mu_2 - \mu_1) H_\varepsilon(\phi) \tag{13}$$

Various geometric quantities such as the unit normal vector and curvature can be easily determined as :

$$n = \frac{\nabla \phi}{|\nabla \phi|} \tag{14}$$

$$\kappa = \nabla . n = \nabla . \frac{\nabla \phi}{|\nabla \phi|} \tag{15}$$

The function δ_ε is used to define quantities having a non 0 value only at the interface (for example interfacial forces). A function F which needs to be distributed on the interface can be distributed on all the domain Ω. Its action is restricted to the interface thanks to the function δ_ε :

$$\int_\Gamma F \simeq \int_\Omega F \ \delta_\varepsilon \tag{16}$$

The evolution of the level set function under the incompressible velocity field u can be modeled by a standard advection equation :

$$\frac{\partial \phi}{\partial t} + u . \nabla \phi = 0 \tag{17}$$

Finally, to ensure the property of the distance function ($|\nabla \phi| = 1$) , we solve the following classical Hamilton-Jacobi equation:

$$\begin{cases} \frac{\partial \phi}{\partial \tau} + s(\phi)(|\nabla \phi| - 1) = 0 \\ \phi(\tau = 0, x) = \phi(t, x) \end{cases} \tag{18}$$

where s represents the signed function.

It is important to remind that the choice of using a fully Eulerian framework is important in the context of the Stratobus project. Indeed, not only it gives a simple access to heat transfer through convection and conduction, but also to fluid-solid interaction through turbulent flows and aerodynamic forces. Therefore, the use of the level set function that separates each subdomain is determining in our case and needs to be extended to the use of membrane interfaces. Finally, the use of anisotorpic mesh adaptation plays an important role[24, 25, 26, 27, 28, 29], both to capture accuratly the interface, to refine near high gradients of the velocity field and to render accurate boundary layers [**?**]. We will not treat this part in this report.

3 Membrane model

Inspired from biomechanics applications, we studied how to implement the additional forces to deal with the interaction between a fluid and an immersed vesicle. In the particular case of vesicle, it is shown in [7] that we need to treat two main proprieties:

• **Bending energy** : to bend the membrane, a bending energy has to be considered

• **Local inextensibility** : the perimeter of the membrane should be the same all the time.

3.1 Bending Force

Starting from the energy that costs to bend a membrane, Helfrich and Canham [30] introduced the following expression:

$$E_c = \int_\Gamma \frac{k_b}{2}\kappa^2 \tag{19}$$

With k_b the bending modulus of the membrane and κ the curvature of the interface. The functional derivative of the expression (19) as taken in [31] leads to the following bending force:

$$F_c = \kappa_b \nabla . \left(\frac{-\kappa^2}{2} \frac{\nabla \phi}{|\nabla \phi|} + \frac{1}{|\nabla \phi|} \left(\mathbb{I}_d - \frac{\nabla \phi \bigotimes \nabla \phi}{|\nabla \phi|^2} \right) \nabla \left\{ |\nabla \phi| \, \kappa \right\} \right) \delta_\varepsilon \nabla \phi \tag{20}$$

Where $P = \left(\mathbb{I}_d - \frac{\nabla \phi \bigotimes \nabla \phi}{|\nabla \phi|} \right)$ is the orthogonal projector ($\mathbb{I}$ is the identity tensor) that can be also rewritten with the normal unit vector as : $P = \mathbb{I} - n \bigotimes n$.

3.2 Inextensibility Force

To complete this particular situation for a vesicle membrane, an inextensibility force must be computed. Many models have been established either through a Lagrange multiplier as in [32, 33] or a direct elastic force as in [34, 35]. This force derives from an elastic energy. It has shown in [34] that the elastic energy depends on the gradient modulus of ϕ. This latter can record an important information of the membrane which is the stretching (on the variation of the surface area). Indeed, a mathematical proof has been given, shown that when the membrane is stretched, the fluid tends to pull in the perpendicular direction of the stretching. These leads to a variation of $|\nabla \phi|$. Figure 3 taken from [36] can explain in a simple manner the principle.

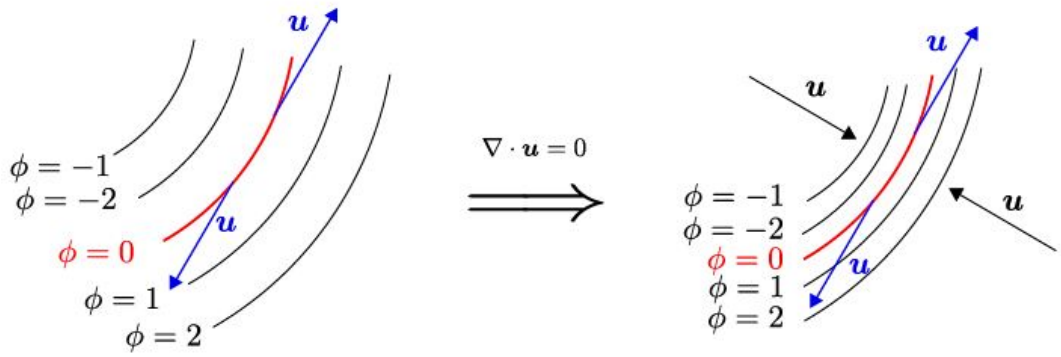


Figure 3: Principle of the inextensibility by elastic force [36]

Thus the elastic energy is defined as :

$$E_{el} = \int_{\Omega} E(|\nabla\phi|)\delta_{\varepsilon} \tag{21}$$

Differentiating the above energy gives the expression of the elastic force

$$F_{el} = \left\{ \nabla E^{'}(|\nabla\phi|) - \nabla . \left[E^{'}(|\nabla\phi|) \frac{\nabla\phi}{|\nabla\phi|} \right] \frac{\nabla\phi}{|\nabla\phi|} \right\} \delta_{\varepsilon} \tag{22}$$

Where $E(|\nabla\phi|)$ stands for a constitutive law for the membrane. Note that $E(1) = 0$ means there is no initial stretching. Taken the most of the time as a linear law $E' = \Lambda\,(|\nabla\phi| - 1)$, it was shown that $E' = \Lambda\ max\,(|\nabla\phi| - 1)$ is an appropriate choice avoiding numerical oscillations. Λ represents the stiffness of the membrane that has to be taken quite large enough to enforce constant area.

Two important points should be mentioned at the end of this section. The first one is that the bending force can introduce numerical problems. Indeed, the level set ϕ need to be derived four times since we have the divergence of the gradient of the divergence of the normal, where the normal itself is written as $n = \frac{\nabla\phi}{|\nabla\phi|}$. To overcome this problem, a state of the art on different techniques have been presented in the next section and will form the perspectives of this initial work. The second point is that, since the stretching is recorded in ϕ, one needs to keep the information of the $\nabla\phi$. As explained previously, the reinitialization resets $\nabla\phi$ to 1, the stretching information will be then lost. Therefore, we need to account for this information through the resolution of the following advection equation with a source term that uses $e = |\nabla\phi|$ before the reinitialization step:

$$\partial_t e + u.\nabla e = -e(n \otimes n) : D(u) \tag{23}$$

3.3 Discretization

The total force localized on the membrane needs now to be transformed to a volume force. Therefore, as mentioned before, we refer to the use of a Dirac function.

Thus, the variational formulation of each force that are added and implemented in the Navier-Stokes equations reads:

$$F_c = \int_\Omega \kappa_b \nabla . \left(\frac{-\kappa^2}{2} \frac{\nabla \phi}{|\nabla \phi|} + \frac{1}{|\nabla \phi|} \left(\mathbb{I}_d - \frac{\nabla \phi \otimes \nabla \phi}{|\nabla \phi|^2} \right) \nabla \left\{ |\nabla \phi| \, \kappa \right\} \right) \delta_\varepsilon \nabla \phi . v \tag{24}$$

$$F_{el} = \int_\Omega \left\{ \nabla E^{'}(|\nabla \phi|) - \nabla . \left[E^{'}(|\nabla \phi|) \frac{\nabla \phi}{|\nabla \phi|} \right] \frac{\nabla \phi}{|\nabla \phi|} \right\} \delta_\varepsilon \cdot v \tag{25}$$

The total force F can be written as $F = F_c + F_{el}$.

4 Numerical experiments

4.1 Flow past a 3D airship

In the first numerical test case, the aim is to assess the capability of our numerical method to simulate the turbulent flow past a complex 3D geometry, namely the Stratobus. We seek also to evaluate the drag and lift forces using an inlet velocity of 25m/s, yielding a span-based Reynolds number of $Re = 10^7$.

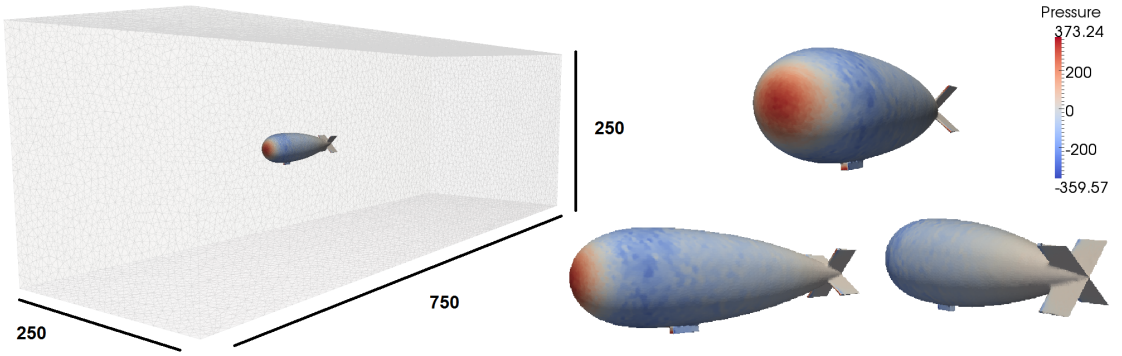


Figure 4: The immersed airship inside a wind channel (left) and the variation of the pressure field (right)

The model is placed in a computational domain of length $50m$ and width $250m \times 250m$. Flat velocity and turbulent viscosity ($\tilde{\nu} = 3\nu$) profiles are prescribed at the inlet boundary, a pressure condition is imposed at the outlet, and slip conditions are used on the boundaries parallel to the flow. At the airship wall, no-slip boundary conditions for the velocity as well as homogeneous Dirichlet conditions for the turbulent viscosity $\tilde{\nu}$ are specified. Again, time marching is performed until the steady-state is reached. The non-dimensional time step is set to $\Delta t = 10^{-3}$. Figure 4 gives a general view of the computational domain.

Recall that the airship is simulated at zero angle of attack. The mesh is pre-adapted at the interface and consists of 1283925 elements and 228210 nodes. The expected pressure distribution is depicted also in Figure 4. The evolution in time of the velocity field until it reaches a steady-state is shown in Figure 5. We can clearly

notice the flow detachement and the wake past the airship. Both the nacelle and the rear airfoils play also a role on the overall nature of the flow.

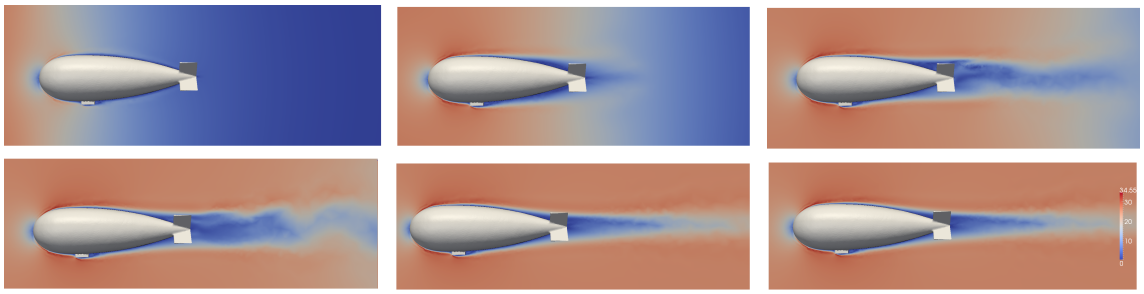


Figure 5: Evolution in time for the velocity field

Results obtained for the drag and the lift are presented in Figures 6 and 7. Qualitatively, the result for the drag is in the expected range obtained in previous setup using different codes at Thales Alenia Space. This first framework is satisfying to proceed further experiments such as different angle of attacks for stability, aerothermal problem and aeroelasticity problem. Moreover, adaptive mesh refinement in 3D is needed to guarantee an accurate resolution of the boundary layer. Therefore, the work of [37] on anisotropic meshing for boundary layers will be used to pursue this analysis.

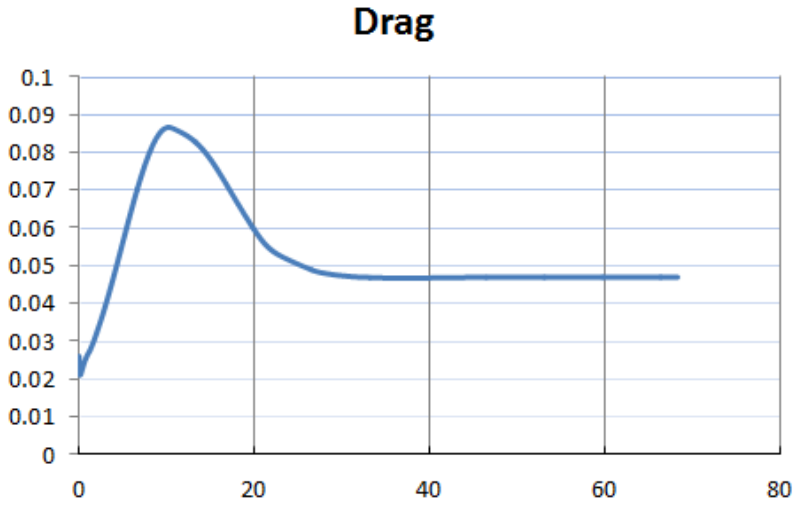


Figure 6: The evolution of the drag coefficient

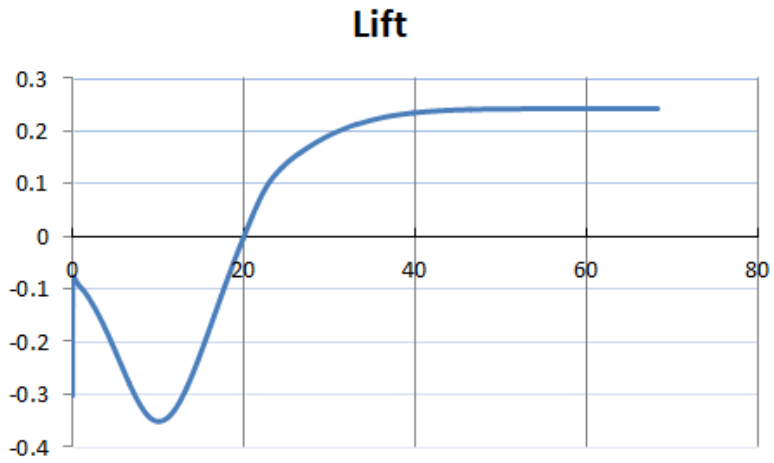


Figure 7: The evolution of the lift coefficient

4.2 Fluid-membrane test case

To test the first implementation of the fluid-membrane model, we will study the test case proposed recently in [38] on the equilibrium shape of a membrane in a fluid at rest. Other PhD works have been solely concentrated to solve this problem [39, 40] using a Lattice Boltzmann method and the Boundary Integral Method.

The membrane, is placed in a fluid at rest in a shape which does not minimize the Helfrich energy. The bending force, expressed above with the geometric parameter of the membrane, causes the motion of the fluid until it reaches its equilibrium shape.

The final shape depends on a dimensionless parameter called the reduced area η. The latter is the ratio between the area of the vesicle and the area of a disk having the same perimeter :

$$\eta = \frac{4\pi A}{p_{er}^2} \tag{26}$$

A is the area of the vesicle and p_{er} its perimeter. This parameter allows us to determine how much the membrane can be deformed.

We show first in Figures 8 to 10 the level set function for the membrane, the obtained Dirac function and we compare it to the reference solution obtained by [38] at different time steps.

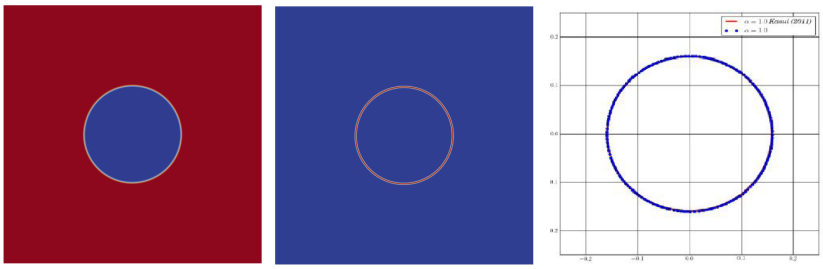


Figure 8: Level set function, Dirac function and the reference solution for $\eta = 1$

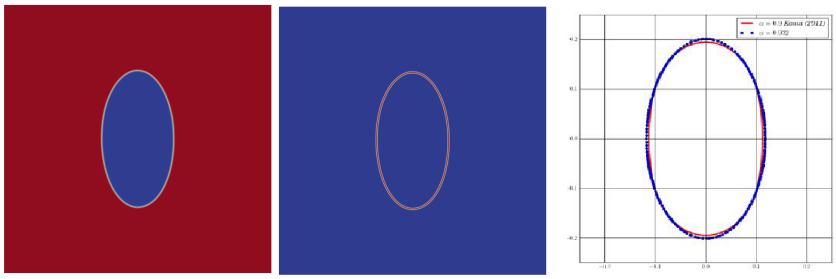


Figure 9: Level set function, Dirac function and the reference solution for $\eta = 0.9$

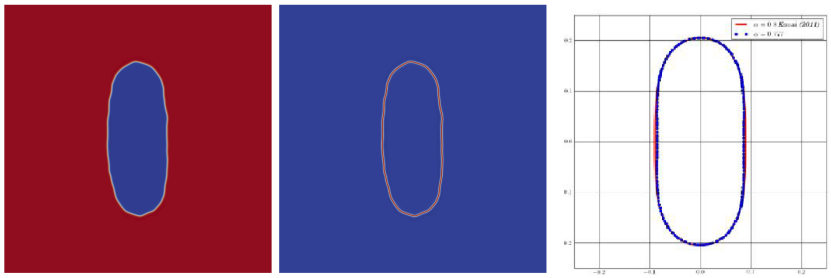


Figure 10: Level set function, Dirac function and the reference solution for $\eta = 0.77$

In Figures 11 to 13 we highlight also the obtained bending and elastic forces at different time steps. We can clearly notice the concentration of these values at the interface, that once are inserted in the Navier-Stokes equations, will steer the velocity field to bend or stretch the membrane, which in return will advect the level set function. Moreover, we can notice the appearance of small perturbations at the last step which is due to the repetition of the projection operations. We discuss this matter in Section 5.

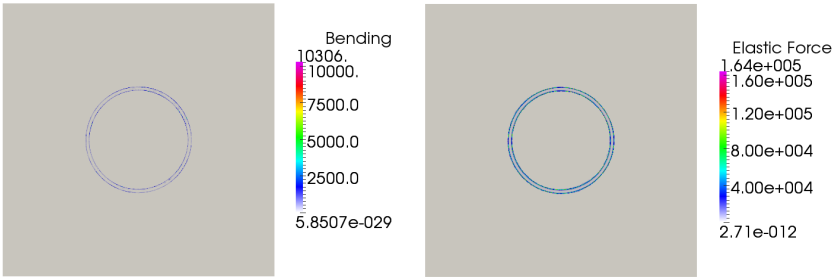


Figure 11: The bending and the elastic forces for $\eta = 1$

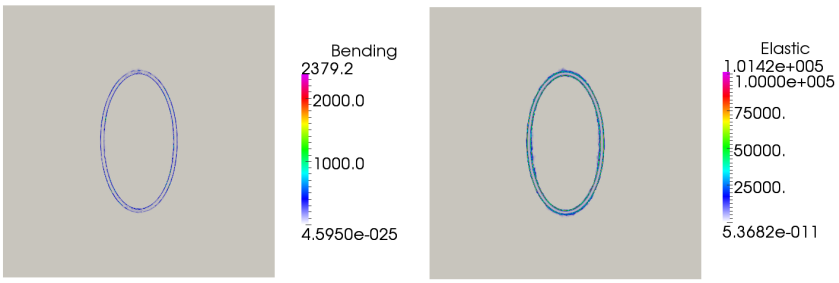


Figure 12: The bending and the elastic forces for $\eta = 0.9$

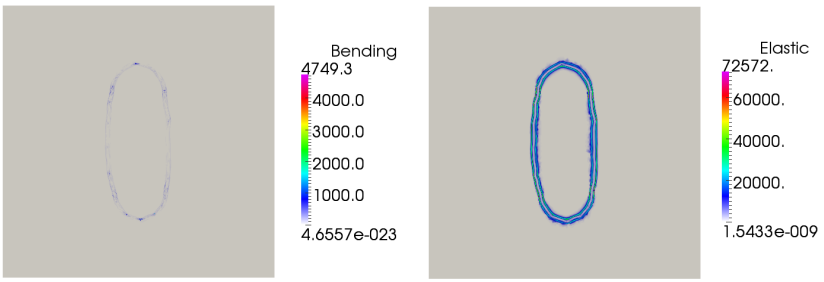


Figure 13: The bending and the elastic forces for $\eta = 0.77$

Finally, Figures 14 to 16 shows the pressure distribution, the obtained velocity field and the adapted mesh highlighting the effects of the implemented forces. The solutions are free from numerical oscillations, which highlight the role of the stabilized finite element methods used here (SUPG for the level set function and VMS for the Navier-Stokes equations).

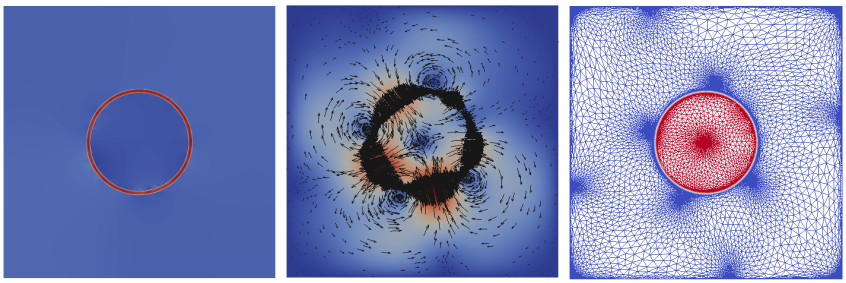


Figure 14: The pressure, velocity and the adapted mesh obtained for $\eta = 1$

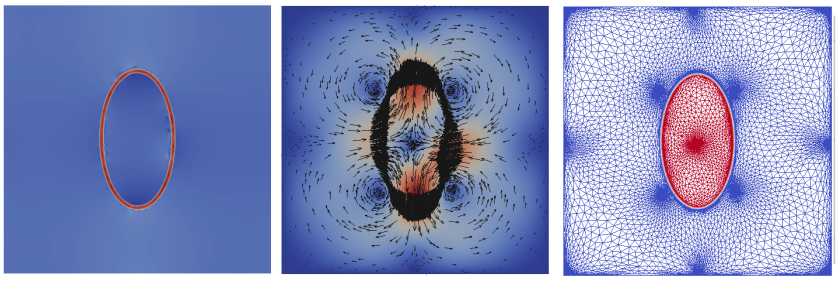


Figure 15: The pressure, velocity and the adapted mesh obtained for $\eta = 0.9$

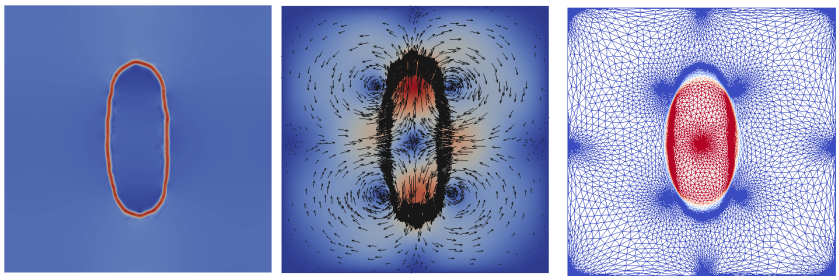


Figure 16: The pressure, velocity and the adapted mesh obtained for $\eta = 0.77$

Despite the numerical issues related to the recovery of high order derivatives, the results remain in good agreement highlighting the potential of the implemented method. Recall also that the numerical techniques used in this work are very different from those used to obtain the reference solution. Table 1 summarizes some of them.

	Reference work [36]	Present work
Disrectization	Finite Difference	Linear Finite Element
Mesh	Structured	Unstructured
Type of mesh	isotropic	Anisotropic
Navier-Stokes resolution	de-coupled	Mixed (v,p)
Gradient recovery	High order method	Simple projection

Table 1: Comparative table

The following step will be naturally to test it in 3D using the hull of the airship while recovering the physical parameters of the envelope from Thales Alenia Space. Indeed, the envelope of the Stratobus may present similar behavior in bending but not in inexensibility. However, the implementation of additional forces in Navier-Stokes and the proposed global algorithm will not change. Moreover, the use of the new implemented unified compressible-incompressible solver in Cimlib (see [41]) will be crucial for the following simulation.

5 High order derivative by smooth projections

Different strategies are developed to be able to get a value of the derivatives of the curvature. We used in our case the L2 double projection. This is already included in our model and should work satisfactorily. However, for higher derivative, repeating this operation will induce small oscillations at the interface that increases in amplitude and lead to important oscillations (as seen in the curvature of figure 17(a)) making the derived field impossible to derive once again. In [42], the authors worked on this subject and proposed a new high order derivative by smooth projection. The idea of the method is to add artificial diffusion to the projection to minimize the oscillations happening when deriving a variable discretized on a low order polynomial set. It adds a small term proportional to Δg which smooths the oscillations and makes the obtained derivative possible to derive as shown in Figure

17(b). The continuous formulation of such a smoothed projection, after integrating by part is the following, for a given $u \in H^1(\Omega)$, find $g \in [H^1(\Omega)]^d \cap [C^0]^d$ so that $\forall v \in [H^1(\Omega)]^d$:

$$\int_\Omega g.v + \int_\Omega \varepsilon_1 \nabla g : \nabla v - \int_{\partial\Omega} \varepsilon_1 (\nabla g n).v = \int_\Omega \nabla u.v \tag{27}$$

with ε_1 a sufficiently small parameter. To be precise, $\nabla g n$ is the classical product of the matrix ∇g and the vector n, thus it is a vector.

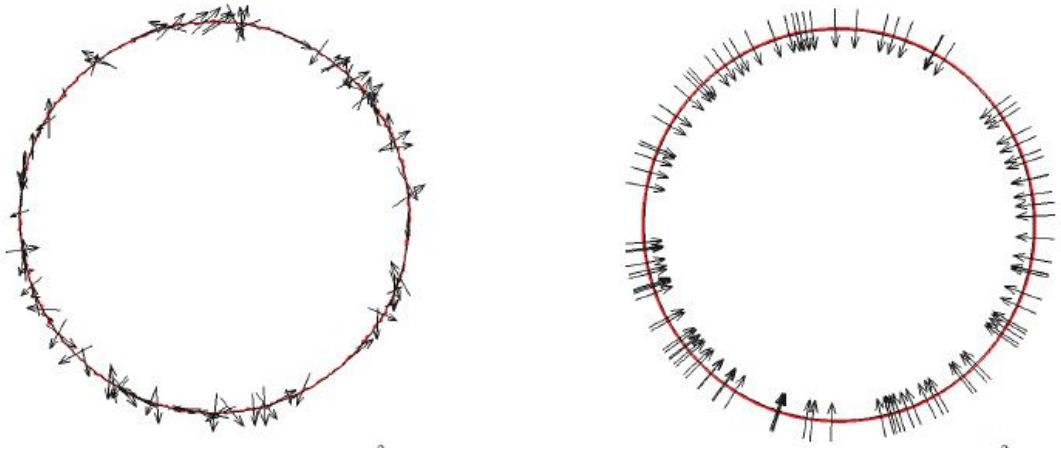


Figure 17: Comparaison between the previous projection and the new one [36]

Again, this step is crucial to simulate accurate fluid-membrane interaction using a level set approach and will be the first subject of further investigations.

6 Conclusion

We have presented a full Eulerian approach to deal with the aerodynamic performance and stability of a new designed airship. It consists first on setting the needed fluid solvers (Navier-Stokes equations coupled to a Spallart almaras turbulent model), then on a geometric representation through a level set method that separates each phase: external air, membrane and internal gaz. Finally, we extended this framework to embed a fluid-membrane model through interfacial forces. This model consists on implementing bending and inextensibility forces and adding them to the Navier-sotek equations. The framework was tested first in 3D to analyze the flow past a fixed airship and compute the aerodynamic forces. Then a fluid-membrane benchmark was chosen to validate the implementation. This work allows us to highlight several numerical challenges: first, the implementation of a high order derivative using smooth projection is needed to ensure free-oscillation forces, then the use of an unified compressible-incompressible solver to take into account the internal gaz of the the airship, finally, the analysis of the envelop proposed by Thales Alenia Space to deduce the physical parameters for our fluid-membrane model.

References

[1] W. Helfrich, "Elastic properties of lipid bilayers: theory and possible experiments," *Zeitschrift für Naturforschung C*, vol. 28, no. 11-12, pp. 693–703, 1973.

[2] L. Miao, U. Seifert, M. Wortis, and H.-G. Döbereiner, "Budding transitions of fluid-bilayer vesicles: The effect of area-difference elasticity," *Physical Review E*, vol. 49, no. 6, p. 5389, 1994.

[3] U. Seifert, K. Berndl, and R. Lipowsky, "Shape transformations of vesicles: Phase diagram for spontaneous-curvature and bilayer-coupling models," *Physical Review A*, vol. 44, no. 2, p. 1182, 1991.

[4] M. Abkarian, C. Lartigue, and A. Viallat, "Tank treading and unbinding of deformable vesicles in shear flow: determination of the lift force," *Physical review letters*, vol. 88, no. 6, p. 068103, 2002.

[5] K. De Haas, C. Blom, D. Van den Ende, M. Duits, and J. Mellema, "Deformation of giant lipid bilayer vesicles in shear flow," *Physical Review E*, vol. 56, no. 6, p. 7132, 1997.

[6] V. Kantsler and V. Steinberg, "Transition to tumbling and two regimes of tumbling motion of a vesicle in shear flow," *Physical review letters*, vol. 96, no. 3, p. 036001, 2006.

[7] G.-H. Cottet and E. Maitre, "Approche eulérienne et méthodes level-set pour l'interaction fluide-structure," in *Séminaire GAMNI de Mécanique des Fluides Numérique*, (Paris, France), Jan. 2007.

[8] D. Salac and M. Miksis, "A level set projection model of lipid vesicles in general flows," *Journal of Computational Physics*, vol. 230, pp. 8192–8215, Sept. 2011.

[9] D. Salac and M. J. Miksis, "Reynolds number effects on lipid vesicles," *Journal of Fluid Mechanics*, vol. 711, pp. 122–146, 2012.

[10] V. Doyeux, Y. Guyot, V. Chabannes, C. Prud'Homme, and M. Ismail, "Simulation of two-fluid flows using a finite element/level set method. application to bubbles and vesicle dynamics," *Journal of Computational and Applied Mathematics*, vol. 246, pp. 251–259, 2013.

[11] E. Hachem, S. Feghali, T. Coupez, and R. Codina, "A three-field stabilized finite element method for fluid-structure interaction: elastic solid and rigid body limit," *International Journal for Numerical Methods in Engineering*, vol. 104, no. 7, pp. 566–584, 2015.

[12] E. Hachem, G. Jannoun, J. Veysset, M. Henri, R. Pierrot, I. Poitrault, E. Massoni, and T. Coupez, "Modeling of heat transfer and turbulent flows inside industrial furnaces," *Simulation Modelling Practice and Theory*, vol. 30, pp. 35–53, 2013.

[13] S. Brogniez, C. Farhat, and E. Hachem, "A high-order discontinuous galerkin method with lagrange multipliers for advection–diffusion problems," *Computer Methods in Applied Mechanics and Engineering*, vol. 264, pp. 49–66, 2013.

[14] G. Jannoun, E. Hachem, J. Veysset, and T. Coupez, "Anisotropic meshing with time-stepping control for unsteady convection-dominated problems," *Applied Mathematical Modelling*, vol. 39, no. 7, pp. 1899–1916, 2015.

[15] P. R. Spalart and S. R. Allmaras, "A one equation turbulence model for aerodinamic flows.," *AIAA journal*, vol. 94, 1992.

[16] A. N. Brooks and T. J. Hughes, "Streamline upwind/petrov-galerkin formulations for convection dominated flows with particular emphasis on the incompressible navier-stokes equations," *Computer methods in applied mechanics and engineering*, vol. 32, no. 1, pp. 199–259, 1982.

[17] A. Ern and J.-L. Guermond, *Theory and practice of finite elements*, vol. 159. Springer Science & Business Media, 2013.

[18] T. J. Hughes, "Multiscale phenomena: Green's functions, the dirichlet-to-neumann formulation, subgrid scale models, bubbles and the origins of stabilized methods," *Computer methods in applied mechanics and engineering*, vol. 127, no. 1, pp. 387–401, 1995.

[19] E. Hachem, B. Rivaux, T. Kloczko, H. Digonnet, and T. Coupez, "Stabilized finite element method for incompressible flows with high reynolds number," *Journal of Computational Physics*, vol. 229, no. 23, pp. 8643–8665, 2010.

[20] R. A. Khurram, Y. Zhang, and W. G. Habashi, "Multiscale finite element method applied to the spalart–allmaras turbulence model for 3d detached-eddy simulation," *Computer Methods in Applied Mechanics and Engineering*, vol. 233, pp. 180–193, 2012.

[21] J. A. Sethian, "Analysis of flame propagation," tech. rep., Lawrence Berkeley Lab., CA (USA), 1982.

[22] J. A. Sethian *et al.*, "Level set methods and fast marching methods," *Journal of Computing and Information Technology*, vol. 11, no. 1, pp. 1–2, 2003.

[23] S. Osher and R. Fedkiw, *Level set methods and dynamic implicit surfaces*, vol. 153. Springer Science & Business Media, 2006.

[24] Y. Mesri, H. Digonnet, and T. Coupez, "Hierarchical adaptive multi-mesh partitioning algorithm on heterogeneous systems," in *Parallel Computational Fluid Dynamics 2008*, pp. 299–306, Springer, 2010.

[25] Y. Mesri, J.-M. GRATIEN, O. M. Ricois, R. Gayno, *et al.*, "Parallel adaptive mesh refinement for capturing front displacements: Application to thermal eor processes.," in *SPE Reservoir Characterization and Simulation Conference and Exhibition*, Society of Petroleum Engineers, 2013.

[26] Y. Mesri, H. Guillard, and T. Coupez, "Automatic coarsening of three dimensional anisotropic unstructured meshes for multigrid applications," *Applied Mathematics and Computation*, vol. 218, no. 21, pp. 10500–10519, 2012.

[27] Y. Mesri, *Gestion et contrôle des maillages non structurés anisotropes: applications en aérodynamique*. PhD thesis, École doctorale Sciences fondamentales et appliquées (Nice), 2007.

[28] Y. Mesri, M. Khalloufi, and E. Hachem, "On optimal simplicial 3d meshes for minimizing the hessian-based errors," *Applied Numerical Mathematics*, vol. 109, pp. 235–249, 2016.

[29] A. Dervieux, Y. Mesri, F. Alauzet, A. Loseille, L. Hascoët, and B. Koobus, "Continuous mesh adaptation models for cfd," *CFD Journal*, vol. 12, no. 3, 2008.

[30] P. B. Canham, "The minimum energy of bending as a possible explanation of the biconcave shape of the human red blood cell," *Journal of Theoretical Biology*, vol. 26, no. 1, pp. 61–81, 1970.

[31] E. Maitre, C. Misbah, P. Peyla, and A. Raoult, "Comparison between advected-field and level-set methods in the study of vesicle dynamics," *Physica D: Nonlinear Phenomena*, vol. 241, no. 13, pp. 1146–1157, 2012.

[32] T. Biben and C. Misbah, "Tumbling of vesicles under shear flow within an advected-field approach," *Physical Review E*, vol. 67, no. 3, p. 031908, 2003.

[33] A. Laadhari, C. Misbah, and P. Saramito, "On the equilibrium equation for a generalized biological membrane energy by using a shape optimization approach," *Physica D: Nonlinear Phenomena*, vol. 239, no. 16, pp. 1567–1572, 2010.

[34] G.-H. Cottet and E. Maitre, "A level set method for fluid-structure interactions with immersed surfaces," *Mathematical models and methods in applied sciences*, vol. 16, no. 03, pp. 415–438, 2006.

[35] T. Milcent, *Une approche eulérienne du couplage fluide-structure, analyse mathématique et applications en biomécanique*. PhD thesis, Université Joseph-Fourier-Grenoble I, 2009.

[36] V. Doyeux, *Modelisation et simulation de systemes multi-fluides. Application aux ecoulements sanguins*. PhD thesis, Université de Grenoble, 2014.

[37] L. Billon, Y. Mesri, and E. Hachem, "Anisotropic boundary layer mesh generation for immersed complex geometries," *Engineering with Computers*, 2016.

[38] V. Doyeux, *Modelisation et simulation de systemes multi-fluides. Application aux ecoulements sanguins*. phdthesis, Université de Grenoble, Jan. 2014.

[39] B. Kaoui, *Modélisation de vésicules en géométrie étendue et dans des systemes micro-fluidiques*. PhD thesis, Grenoble 1, 2009.

[40] B. Kaoui, J. Harting, and C. Misbah, "Two-dimensional vesicle dynamics under shear flow: Effect of confinement. pre, 83 (6): 066319–+," 2011.

[41] E. Hachem, M. Khalloufi, J. Bruchon, R. Valette, and Y. Mesri, "Unified adaptive variational multiscale method for two phase compressible-incompressible flows," *Computer Methods in Applied Mechanics and Engineering*, vol. 308, pp. 238–255, 2016.

[42] A. Laadhari, *Modelisation numérique de la dynamique des globules rouges par la méthode des fonctions de niveau*. PhD thesis, Grenoble, 2011.